Preparation and properties of calcium silicate hydrate-poly(vinyl alcohol) nanocomposite materials

Mojumdar, S. C.; Raki, L.

Publisher's version / Version de l'éditeur:
https://doi.org/10.1007/s10973-005-0846-8
Journal of Thermal Analysis and Calorimetry, 82, 1, pp. 89-95, 2005-09-01

Preparation and properties of calcium silicate hydrate-poly(vinyl alcohol) nanocomposite materials

NRCC-48686

Mojumdar, S.C.; Raki, L.

A version of this document is published in / Une version de ce document se trouve dans : Journal of Thermal Analysis and Calorimetry, v. 82, no. 1, Sept. 2005, pp. 89-95 doi: 10.1007/s10973-005-6837-y

Journal of Thermal Analysis and Calorimetry, Vol. 82 (2005) 89–95

PREPARATION AND PROPERTIES OF CALCIUM SILICATE HYDRATE–POLY(VINYL ALCOHOL) NANOCOMPOSITE MATERIALS

S. C. Mojumdar and L. Raki*

Institute for Research in Construction, National Research Council of Canada, M-20, 1200 Montreal Road, Ottawa Ontario K1A 0R6, Canada

A series of calcium silicate hydrate (C–S–H)-polymer nanocomposite (C–S–HPN) materials were prepared by incorporating poly(vinyl alcohol) (PVA) into the inorganic layers of C–S–H during precipitation of quasicrystalline C–S–H from aqueous solution. The as synthesized C–S–HPN materials were characterized by Fourier-transform infrared photoacoustic (FTIRPAS) spectroscopy, X-ray diffraction (XRD), scanning electron microscopy/energy dispersed spectroscopy (SEM/EDS), thermogravimetric analysis (TG), differential thermogravimetry (DTG) and differential scanning calorimetry (DSC). The XRD peaks of C–S–HPN materials suggest the intermediate organizations presenting both intercalation of PVA and exfoliation of C–S–H. The SEM micrographs of C–S–H, PVA and C–S–HPN materials with different PVA contents exhibit the significant differences in their morphologies. Effects of the material compositions on the thermal stability of a series of C–S–HPN materials along with PVA and C–S–H were studied by TG, DTG and DSC. Three significant decomposition temperature ranges were observed in the TG curves of all C–S–HPN materials.

Keywords: *C–S–H, DSC, DTG, FTIRPAS spectroscopy, nanocomposite, PVA, SEM, TG, XRD*

Introduction

Nanocomposites are a new class of composites, that are particle-filled polymers for which at least one dimension of the dispersed particles is in the nanometer range. Three types of nanocomposites, depending on how many dimensions of the dispersed particles are in the nanometer range can be distinguished [1]. Particles with three dimensions in the order of nanometers are typically isodimensional, such as spherical silica nanoparticles obtained by in situ sol–gel methods [2, 3] or by polymerization promoted directly from their surface [3, 4]. They also include semiconductor nanoclusters [5] and others [3]. Nanotubes or whiskers (with dimensions in the nanometer scale and the third forming a larger elongated structure), for example, carbon nanotubes [6] or cellulose whiskers [7, 8], are extensively studied as reinforcing phases yielding materials with exceptional properties. The third type of nanocomposites is characterized by only one dimension in the nanometer range. In this case the material is present in the form of sheets of one to a few nanometers thick and hundreds to thousands nanometers long. This family of composites is referred to as polymer-layered crystal nanocomposites.

Depending on the nature of the components used (layered structure, organic ions/polymer matrix) and the method of preparation, three main types of composites may be obtained when a layered structure is associated with a polymer [1].

If the polymer is unable to intercalate between the layered sheets, a phase-separated composite is obtained, whose properties stay in the same range as traditional microcomposites. Beyond this classical family of composites, two types of nanocomposites can be distinguished. An 'intercalated' structure in which a single (and sometimes more than one) extended polymer chain is intercalated between the inorganic layers resulting in a well-ordered multilayer morphology built up with alternating polymeric and inorganic layers. When the layers are completely and uniformly dispersed in a continuous polymer matrix, an 'exfoliated or delaminated' structure is obtained. XRD together with TEM/SEM are usually used to identify intercalated structures. In such nanocomposites, the repetitive multilayer structure is well preserved, allowing the interlayer spacing to be determined. The intercalation of the polymer chains usually increases the interlayer spacing, in comparison with the spacing of the host used, leading to a shift of the diffraction peak towards lower angle values (angle and layer spacing values being related through the Bragg's relation: $\lambda=2d\sin\theta$, where λ corresponds to the wave length of the X-ray radiation used in the diffraction experiment, d is the spacing between diffractional lattice planes and θ is the measured diffraction angle or glancing angle).

* Author for correspondence: Subhash.Mojumdar@nrc-cnrc.gc.ca

1388–6150/$20.00

Akadémiai Kiadó, Budapest, Hungary
Springer, Dordrecht, The Netherlands

As far as exfoliated structure is concerned, no more diffraction peaks are visible in the XRD diffractograms either because of a much too large spacing between the layers (i.e. exceeding 8 nm in the case of ordered exfoliated structure) or because the nanocomposite does not present ordering anymore. Other intermediate organizations can exist presenting both intercalation and exfoliation. In this case, a broadening of the diffraction peak is often observed [1].

Organic–inorganic hybrid materials, composed of layered inorganic matrix with organic polyconjugated macromolecules in the interlayer space, have been the subjects of thorough attention of researchers for the past 5–15 years [9–39]. One of the very important materials of this type is so called macro-defect-free (MDF) material at microscopic and nanometric levels [40]. Polymers are very important additives in the manufacture and processing of various materials, where the modification of interfaces and particles surface functionalisations are largely influenced by the model of functional polymer. The theory of functional polymer, modification of a surface by grafting/reaction of polymer chains to/with the surface of and inorganic materials are discussed in [41, 42].

Calcium silicates hydrates (C–S–H) are the main hydrated phases in cement paste. They have a nanocrystalline structure and possess hydraulic properties. Nanocomposite materials consisting of inorganic nanolayers of C–S–H and organic polymers have evoked intense research interest lately because their unique characteristics create many potentially commercial applications. The synthesis of C–S–H-based nanocomposites using a number of organic polymers was recently reported in [19, 21, 23]. Poly(vinyl alcohol) (PVA) was intercalated into C–S–H structure at higher Ca/Si ratio mainly as this polymer showed less affinity to low Ca/Si ratios.

Polymer-clay, nanocomposite materials are reported to promote thermal [43, 44], mechanical [45], molecular barriers [46], flame retardant behavior [47–54] and corrosion protection properties [55–57]. Therefore, their systematic investigation of the reaction possibility of PVA with synthetic C–S–H at low Ca/Si ratio (0.7) as well as to characterize the composite materials by nanotechnological methods are the main interests of this contribution.

Experimental

Materials

Poly(vinyl alcohol) (Sigma Chemical Co., St. Louis, USA), $Na_2SiO_3 \cdot 9H_2O$ (National Silicates, Toronto Canada), $Ca(NO_3)_2 \cdot 4H_2O$ and NaOH (Fisher Scientific, Fair Lawn, New Jersey, USA) were used to synthesize C–S–H and C–S–HPN materials.

Synthesis of C–S–HPN materials

C–S–H and C–S–HPN materials with PVA content of (0.0 and 0.05, 0.15, 0.5 and 0.75 g g^{-1} Ca salt) were synthesized by gradually adding calcium nitrate solution (1 mol L^{-1}) with continual stirring under nitrogen to sodium silicate solution, which was pre-dissolved with PVA (only for the synthesis of C–S–HPN materials) in CO_2-free deionized water. The initial Ca/Si molar ratio was 0.7 for C–S–H and all C–S–HPN materials. The pH value was kept between 13.1–13.4 by adding NaOH solution (4.0 M) during the precipitation of C–S–H. After aging the suspension at 60°C for seven days with continuous stirring, the precipitate was separated by vacuum filtration and washed with CO_2-free deionized water to remove sodium and nitrate ions and any residual PVA. The precipitates were then washed with acetone and dried at 60°C in a vacuum oven for 7 days. C–S–H and C–S–HPN material samples are summarized in Table 1.

Table 1 Synthetic C–S–H and C–S–HPN materials (Ca/Si=0.7)

Materials	PVA content / g g^{-1} Ca salt
C–S–H (0.7)	0.00
C–S–H–PVA (0.7–0.05)	0.05
C–S–H–PVA (0.7–0.15)	0.15
C–S–H–PVA (0.7–0.3)	0.30
C–S–H–PVA (0.7–0.5)	0.50
C–S–H–PVA (0.7–0.75)	0.75

Analytical procedure

The powder X-ray diffraction (XRD) patterns were performed on a Scintag XDS 2000 X-ray diffractometer using CuK_α radiation at 45 kV and 35 mA between 4 and 65° (2θ) with a graphite secondary monochromator.

FTIRPAS spectra were recorded by using a MTEC Model 200 photoacoustic detector. Thermal analyses on powder samples (~20 mg) were carried out using a simultaneous SDT Q600 T.A.I. instrument at 10°C min^{-1} from room temperature (RT) to 1000°C under nitrogen atmosphere using a flowing rate 100 mL min^{-1}.

Scanning electron microscopic and chemical analyses (SEM/EDS) were conducted using a Cambridge Systems Stereoscan 250 instrument equipped with an Oxford Instruments Inca 200 EDS.

Results and discussion

X-ray diffraction analysis

The powder XRD patterns of C–S–H and a series of C–S–HPN materials are presented in Fig. 1. The powder XRD patterns exhibit diffraction peaks at 2θ=5–9° (interlayer spacing d=1.26 nm for C–S–H and 1.27–1.40 nm for C–S–HPN materials). The XRD peaks of C–S–HPN materials (Fig. 1) not only shifted to the lower angle but also broadened. This behavior suggests the intermediate organizations presenting both intercalation and exfoliation. The overall C–S–H layers expansion was small compared to PVA molecules diameter (0.45 nm). The formation of these nanocomposites depends on the structure of the host material itself, the charge density on the surface (here the Ca/Si ratio), the method of preparation (in-situ or exchange), and the type of organic polymers. The small expansion upon intercalation could only be explained by a single linear extension conformation of PVA molecules [19, 21, 23].

The intermediate organizations presenting both intercalation and exfoliation are also confirmed by SEM. The highest intercalation of PVA into the C–S–H was achieved for C–S–HPN materials with PVA 0.5 (g g^{-1} Ca salt) (Fig. 1).

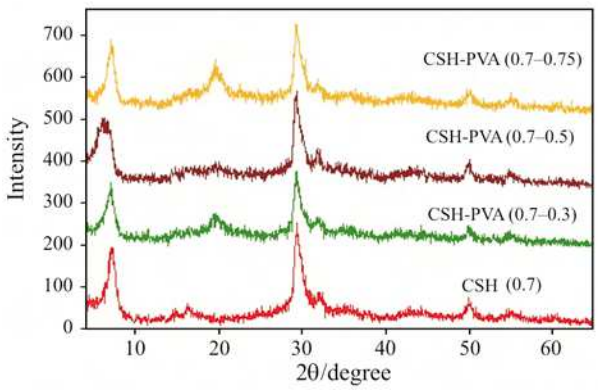

Fig. 1 Powder XRD patterns of C–S–H and C–S–HPN materials with various PVA (g g^{-1} Ca salt) contents

SEM analysis

The SEM images of bulk PVA, C–S–H and C–S–HPN materials are shown on Figs 2–4. Figure 2 represents SEM images of C–S–H (top) and PVA (bottom). For C–S–H, the particles display a sinuous surface, typical of this material [58]. In the case of PVA, the matrix image shows a semi-amorphous character, as it has been confirmed by XRD results (not shown).

A unique example of intercalation of a PVA into the C–S–H layers is presented in Fig. 3. The image exhibits a layered organization of PVA molecules and C–S–H particles. EDS analyses were carried out on several different zones of C–S–H and C–S–HPN. The Ca/Si ratios of C–S–H and C–S–HPN materials confirmed the theoretical expectation.

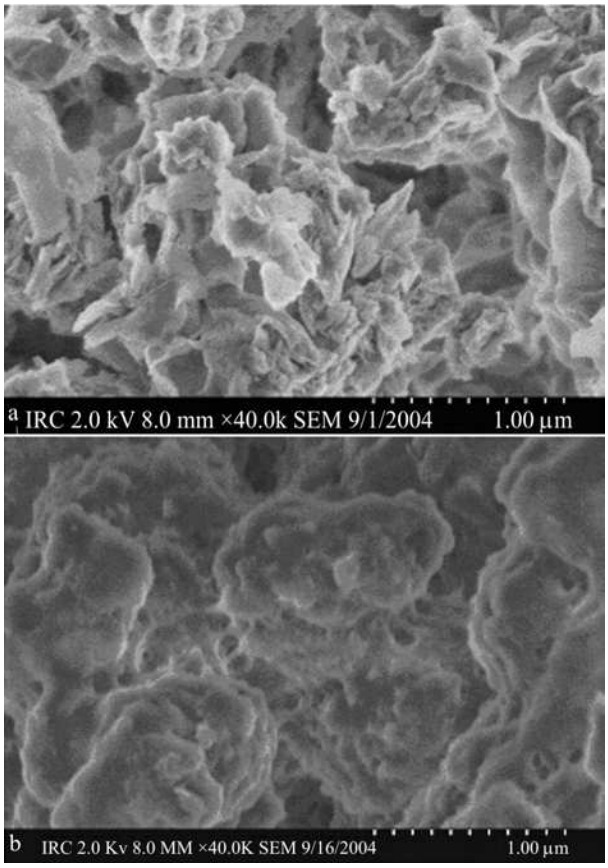

Fig. 2 SEM micrographs of a – synthetic C–S–H and b – pure PVA

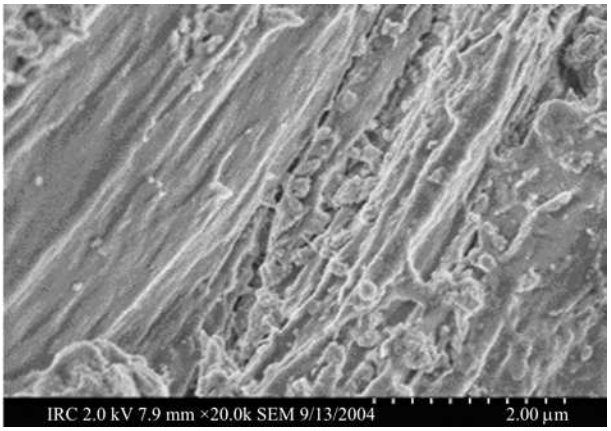

Fig. 3 SEM micrograph of a typical C–S–HPN material: an intercalated PVA fiber between the C–S–H layers

A clear example of two phases C–S–HPN materials is presented in Fig. 4. The light phase has a lower carbon (PVA) content than the dark phase that contains as much as 4x more carbon, as analyzed by EDS. It can be concluded on the basis of SEM, carbon con-

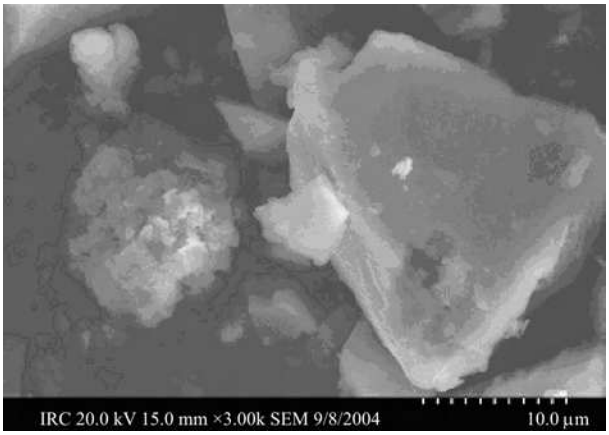

Fig. 4 SEM micrographs of two separate phases: left – intercalated and right – exfoliated of C–S–HPN materials

tent and XRD results that the light phase is the intercalated and the dark phase is the exfoliated C–S–HPN materials. Interfaces of C–S–HPN materials do not exhibit radial boundaries. Significant differences in SEM micrographs of C–S–H, PVA and C–S–HPN materials with different polymer ratios are observed. The result is consistent with the powder XRD results.

FTIRPAS spectral analysis

The most important FTIRPAS spectral bands of C–S–H, bulk PVA and selected C–S–HPN materials are summarized in Table 2. All spectra of C–S–H and C–S–HPN materials contain a characteristic set of bands at the range 972–977 cm^{-1}. These are the most intensive bands in all spectra and can be assigned to Si–O stretching vibration of the Q^2 tetrahedra. The weak bands in the range 811-816 cm^{-1} are present in C–S–H and C–S–HPN materials, and are assigned to Si–O stretching vibrations of the Q^1 tetrahedra. The Si–O–Si bands at 666–673 cm^{-1} have decreased in intensity and increased in width with increasing polymer contents. The bands at 3741–3745 cm^{-1} are due to Si–OH stretching in the isolated Si–OH species. The most striking feature of the C–S–H spectra (not shown) is the decreasing intensity of the bands with increasing polymer contents, suggesting a progressively decreasing concentration of Si–OH group. These are the key information of the structure of C–S–H and C–S–HPN materials. The stretching bands at 3339–3422 cm^{-1} can be attributed to water molecules. This observation is consistent with the observed decrease in water content with increasing polymer contents for these samples. At higher PVA contents, less H_2O molecules can be accommodated within the layer. The bands in the range of 1643–1651 cm^{-1} are due to H–O–H bending vibrations of H_2O molecules. Other bands at 447–474 cm^{-1} are due to the internal deformation of SiO_4 tetrahedra. The bands in the range of 1410–1439 cm^{-1} correspond to the asymmetric stretching (ν_3) of CO_3^{2-} (it is not possible to prevent incorporation of CO_2 during sample preparation) [59].

The characteristic vibration bands of PVA and C–S–HPN materials are shown at 3240–3337 cm^{-1} (–OH), 2925–2936 cm^{-1} (–CH_3), 2857–2891 cm^{-1} (–CH_2), 1410–1445 cm^{-1} (O=C–OR), 1035–1093 cm^{-1} (C–O–C) and 831–844 cm^{-1} (–CH) [60]. Since the stretching vibrations of (O=C–OR) and CO_3^{2-} appear at very close region, these two bands overlapped and become one peak in the spectra of C–S–HPN materials. The presence of PVA bands in C–S–HPN composites is indicative of PVA molecules intercalated between C–S–H sheets, as it is also supported by XRD and SEM results.

Thermal properties of C–S–H, PVA and C–S–HPN materials

The most important thermoanalytical (TG, DTG and DSC) data of C–S–H, representative C–S–HPN mate-

Table 2 Selected FTIRPAS spectral data (4000–400 cm^{-1}) of C–S–H, PVA and C–S–HPN materials

Assignments	C–S–H/cm^{-1}	C–S–H–PVA (0.7–0.05)/cm^{-1}	C–S–H–PVA (0.7–0.30)/cm^{-1}	C–S–H–PVA (0.7–0.5)/cm^{-1}	C–S–H–PVA (0.7–0.75)/cm^{-1}	PVA/cm^{-1}
Si–O	973, 811	974, 812	972, 813	978, 815	977, 816	–
Si–O–Si	670	673	672	666	673	–
Si–OH	3742	3741	3742	3745	3744	–
H–O–H	1645	1643	1650	1651	1651	–
OH	3390	3422, 3240	3394, 3241	3375, 3268	3339, 3281	3337
CH_3	–	2936	2933	2933	2925	2934
CH_2	–	2857	2858	2859	2876	2891
O=C–OR	–	1410	1439	1433	1434	1445
C–O–C	–	1036	1035	1038	1039	1093
CH	–	831	841	842	843	844
CO_3^{2-}	1431	1410	1439	1433	1434	–
other bands	448	460	474	448	447	–

Table 3 Summary of thermal analyses data for C–S–H, PVA and C–S–HPN materials

Compound	T_d/°C	DTG peak/°C	T_g/°C	T_m/°C
C–S–H	250, over 600	86, 645	87	–
C–S–H–PVA (0.7–0.05)	225, 350, 650, over 650	95, 238, 432, 709	98	246
C–S–H–PVA (0.7–0.5)	170, 399, 550, over 550	80, 190, 430	77	199
C–S–H–PVA (0.7–0.75)	195, 250, 550, over 550	95, 223, 431	104	229
PVA	250, 370, 500	278, 431	60	230

T_d – decomposition temperature; T_g – glass transition temperature; T_m – melting temperature

rials and bulk PVA are presented in Table 3. Figure 5 shows the TG curves of mass loss as a function of temperature, under nitrogen, of the C–S–H, PVA and representative C–S–HPN materials in the same figure. There are significant differences in the thermal decomposition properties of C–S–H, PVA and C–S–HPN materials. The mass loss curves of C–S–HPN materials generally lie between C–S–H and PVA; however, with the increasing polymer contents, the TG curves of the C–S–HPN materials shift toward the PVA curve. In general three temperature regions on the TG curves of C–S–H and C–S–HPN materials were observed:

- Region I (rT – 250°C): this is the region of C–S–H decomposition [60–65] due to loss of molecular water with DTG peaks at 80–95°C. In the case of C–S–HPN materials, the decomposition temperature (T_d) in this region is variable depending on the synthesis and material compositions (Table 3, Fig. 5).
- Region II (150–550°C): this temperature region is attributed mainly to the polymeric material decomposition [60–63]. For C–S–HPN materials, two decomposition steps are observed, similar to the decomposition of pure PVA, (Table 3, Fig. 5). DTG curves of C–S–HPN materials as well as PVA exhibit two DTG peaks at the temperature range 190–432°C (Table 3, Fig. 6). The greater the polymer content, the larger the mass losses on the TG curve in this region. This fact strongly suggests the presence of a higher percentage of PVA in the C–S–HPN materials produced with higher polymer contents. The shift of DTG peak to lower temperature (from 278 to 190–238°C) in C–S–HPN materials compared to pure PVA is due to the environmental changes of PVA, which has been resulted from intercalation. Relatively constant DTG peaks temperature at about 431°C corresponds to the thermal decomposition of polymeric structure. These findings are similar to those of MDF materials [62, 63].
- Region III (over 550 °C): this temperature region is characteristic for $CaCO_3$ decomposition [62–69]. Since the amount of $CaCO_3$ (which may formed during the synthesis of C–S–H and C–S–HPN materials) is very low, DTG peaks corresponding to the release of CO_2 from $CaCO_3$ is very weak or insignificant. The atmospheric moisture and CO_2 causes the formation of $Ca(OH)_2$ and $CaCO_3$ according to the reactions 1 and 2.

$$CaO(s)+H_2O(l)=Ca(OH)_2(s) \quad (1)$$

$$Ca(OH)_2(s)+CO_2(g)=CaCO_3(s)+H_2O(l) \quad (2)$$

DSC traces of C–S–H and C–S–HPN materials are presented in Fig. 7. PVA exhibits an endotherm at 60°C corresponding to the glass transition temperature (T_g) of PVA [60–62]. All the C–S–HPN materials

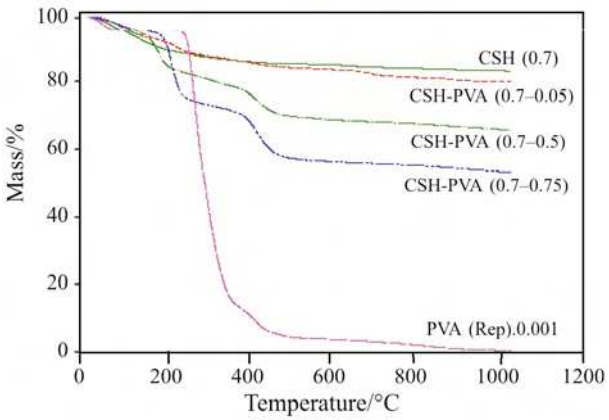

Fig. 5 TG curves of C–S–H, PVA and C–S–HPN materials with different polymer contents

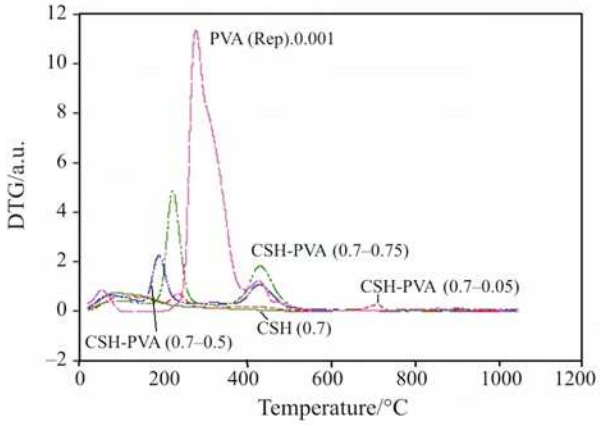

Fig. 6 DTG curves of C–S–H, PVA and C–S–HPN materials with different polymer contents

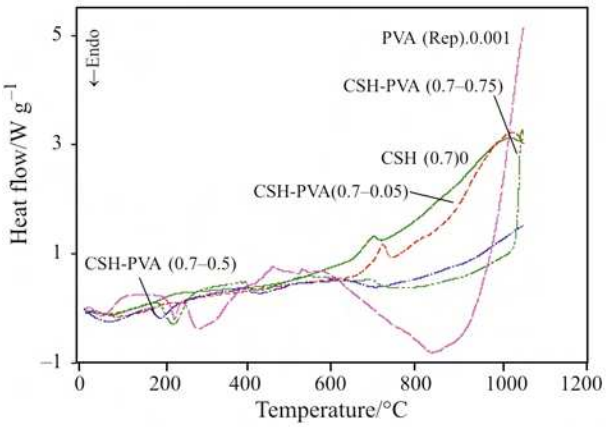

Fig. 7 DSC curves of C–S–H, PVA and C–S–HPN materials with different polymer contents

are found to have a higher (T_g) compared to the bulk PVA, as shown in Table 3 and Fig. 7. This is tentatively attributed to the confinement of the intercalated polymer chains within the C–S–H galleries that prevent the segmental motions of the polymer chains. Another endotherm of bulk PVA at higher temperature (ca. 230°C), corresponding to the crystalline melting point (T_m) of PVA, is also found in DSC curves [60]. This endotherm is absent in the DSC curve of C–S–H but is present in all the DSC curves of C–S–HPN materials. The DSC peaks of C–S–HPN materials shift to lower temperatures suggesting the intercalation of PVA into C–S–H. The larger shift of the endotherm (toward the lower temperature) occurs in the DSC curve of C–S–HPN material containing PVA 0.5 (g g^{-1} Ca salt). This suggest the greatest intercalation of the PVA molecules. This fact is also confirmed by XRD results (d=1.4 nm).

Conclusions

New calcium silicate hydrate/poly(vinyl alcohol) nanocomposites (C–S–HPN) have been prepared and characterized. Synthetic C–S–H and C–S–HPN materials were analyzed by XRD, SEM/EDS, TG, DTG, DSC and FTIRPAS spectra. The XRD and SEM results suggested the occurence of intermediate organizations representing both intercalation and exfoliation in C–S–HPN materials. Significant differences in the morphologies of C–S–H and C–S–HPN materials with different PVA contents have been observed in SEM micrographs. The influence of the material composition on the thermal decomposition of C–S–HPN materials along with the pure PVA and synthetic C–S–H have been studied by TG, DTG and DSC. Three significant decomposition temperature regions were observed in the TG curves of different C–S–HPN samples, corresponding to the decomposition temperature of C–S–H structure, polymeric entities, and $CaCO_3$.

This investigation opens up new routes to develop cement-based nanocomposites for future potential application in the construction field, such as coatings for corrosion protection and for fire retardancy. A study to elucidate the effect of PVA molecules intercalation on Ca/Si ratio of C–S–HPN by means of XRF, MAS NMR and AFM spectroscopy will be presented in a future article.

Acknowledgements

The authors would like to thank Ana Delgado for helping with FTIRPAS spectroscopic measurements and Jim Margeson for performing SEM/EDS analysis.

References

1 M. Alexandre and P. Dubois, Mater. Sci. Eng., 28 (2000) 1.
2 J. E. Mark, Polym. Eng. Sci., 36 (1996) 2905.
3 E. Reynaud, C. Gauthier and J. Perez, Rev. Metall./Cah. Inf. Tech., 96 (1999) 169.
4 T. Von Werne and T. E. Patten, J. Am. Chem. Soc., 121 (1999) 7409.
5 N. Heron and D. L. Thorn, Adv. Mater., 10 (1998) 1173.
6 P. Cavert, Potential application of nanotubes, in: T. W. Ebbesen (Ed.), Carbon Nanotubes, CRC Press, Boca Raton, FL 1997, pp. 277–292.
7 V. Favier, G. R. Canova, S. C. Shrivastava and J. Y. Cavaille, Polym. Eng. Sci., 37 (1997) 1732.
8 L. Chazeau, J. Y. Cavalle, G. Canova, R. Dendievel and B. Boutherin, J. Appl. Polym. Sci., 71 (1999) 1797.
9 M. Delucchi and G. Cerisola, Constr. Build. Mater., 15 (2001) 351.
10 M. G. Kanatzidis and L. M. Tonge, J. Am. Chem. Soc., 109 (1987) 3797.
11 M. Drábik, L. Gáliková, K. G. Varshney and M. A. Quraishi, J. Therm. Anal. Cal., 76 (2004) 91.
12 G. K. D. Pushpalal, J. Mater. Sci., 35 (2000) 981.
13 B. X. Li, W. Q. Liang, W. S. Zhang and Z. He, J. Chin. Cer. Soc., 28 (2000) 325.
14 S. C. Mojumdar, J. Therm. Anal. Cal., 64 (2001) 1133.
15 J. D Birchal, A. J. Howard, K. Kendal and J. H. Raistrick, 1988 June, Cementitious Composition and Cementitious Product of High Flexural Strength. European Pat. Specification, B1, No. 0055035, pp. 1–17.
16 M. Drabik, S. C. Mojumdar and L. Galikova, Cem. Concr. Res., 31 (2001) 751.
17 J. A. Lewis and P. G. Desai, 1996, MAETA Workshop on High Flexural Polymer-Cement Composite, Sakata, 3–4 October, pp. 49–58.
18 S. C. Mojumdar and M. Drabik, Science of cement and concrete-Kurdowski Symposium (Akapit Scientific Publisher, Poland 2001).
19 H. Matsuyama and J. F. Young, J. Mater. Res., 14 (1999) 3379.

20 S. C. Mojumdar, A. Ray, M. Drábik, A. Cigan, F. Hanic and P. Capek, Solid State Phenomena, 90–91 (2003) 365.
21 H. Matsuyama and J. F. Young, J. Mater. Res., 14 (1999) 16.
22 M. Drabik, L. Galikova and S. C. Mojumdar, Key Engineering Materials, 206 (2002) 1867.
23 H. Matsuyama and J. F. Young, Chem. Mater., 11 (1999) 3389.
24 S. C. Mojumdar, Thermophysics 2001, October 23–25, Račková Dolina, High Tatras, Slovakia 2001, pp. 93–98.
25 K. Kendal, A. J. Howard and J. D. Birchal, Philos. Trans. R. Soc., A310 (1983) 139.
26 M. Drábik, S. C. Mojumdar and R. C. T. Slade, Ceramics – Silikaty, 46 (2002) 68.
27 B. X. Li, W. Q. Liang and Z. He, J. Wuhan Univ. Technol., 16 (2001) 25.
28 M. Delucchii and G. Cerisola, Constr. Build. Mater., 15 (2001) 351.
29 S. C. Mojumdar, Challenges for Coord. Chemistry in the new century, 5 (2001) 453.
30 R. Alfani, P. Colombet, A. D'Amore, N. Rizzo and L. Nicolais, J. Mater. Sci., 34 (1999) 5683.
31 C. Y. Rha, J. W. Seong, C. E. Kim, S. K. Lee and W. K. Kim, J. Mater. Sci., 34 (1999) 4653.
32 C. K. Park, J. Cer. Soc. Jap., 106 (1998) 268.
33 J. A. Lewis and M. A. Boyer, Adv. Cem. Bas. Mater., 2 (1995) 2.
34 M. Tan, J. Lu and K. Wu, Cem. Concr. Res., 24 (1994) 1185.
35 P. G. Desai, J. A. Lewis and D. P. Bentz, J. Mater. Sci., 29 (1994) 711.
36 I. A. A. Ibrahim, H. H. ElSersy and M. F. Abadir, J. Therm. Anal. Cal., 76 (2004) 713.
37 J. Dweck, P. F. Ferreira da Silva, R. Silva Aderne, P. M. Büchler and F. K. Cartledge, J. Therm. Anal. Cal., 71 (2003) 821.
38 S. C. Mojumdar, B. Chowdhury, K. G. Varshney and K. Mazanec, J. Therm. Anal. Cal., 78 (2004) 135.
39 T. Lan, P. D. Kaviratna and T. J. Pinnavaia, Chem. Mater., 6 (1994) 573.
40 I. Odler, Special Inorganic Cement, Capter 13.3, MDF cement, E & F. N. Spon, London, New York 2000.
41 G. Wegner, Acta Materialia (The millennium special issue), 48 (2000) 253.
42 M. Drabik and R. C. T. Slade, Interf. Sci., 12 (2004) 375.
43 M. Zanetti, P. Bracco and L. Costa, Polym. Degrad. Stab., 85 (2004) 657.
44 H.-L. Tyan, Y-C. Liu and K-H. Wei, Chem. Mater., 11 (1999) 1942.
45 Z. Wang and T. J. Pinnavaia, Chem. Mater., 10 (1998) 3769.
46 J. Liu, Y. Gao, F. Wang and W. Ming, J. Appl. Polym. Sci., 75 (2000) 384.
47 J. W. Gilman, Appl. Clay Sci., 15 (1999) 31.
48 J. W. Gilman, C. L. Jackson, A. B. Morgan, J. R. Hayyis, E. Manias, E. P. Giannelis, M. Wuthenow, D. Hilton and S. H. Philips, Chem. Mater., 12 (2000) 1866.
49 D. Porter, E. Metcalfe and M. J. K. Thomas, Fire Mater, 24 (2000) 45.
50 J. Wang, J. Dua, J. Zhu and C. A. Wilkie, Polym. Degrad. Stab., 77 (2002) 249.
51 M. Zanetti, G. Camino, D. Canavese, A. B. Morgan, F. J. Lamelas and C. A. Wilkie, Chem. Mater., 14 (2002) 189.
52 M. Zanetti, T. Kashiwagi, L. Falqui and G. Camino, Chem. Mater., 14 (2002) 881.
53 J. Zhu, P. Start, K.A. Mauritz and C. A. Wilkie, Polym. Degrad. Stab., 77 (2002) 253.
54 J. Zhu, F. Uhl, A. B. Morgan and C. A. Wilkie, Chem. Mater., 13 (2001) 4649.
55 J. M. Yeh, S. J. Liou, C. Y. Lai, P. C. Wu and T. Y. Tsai, Chem. Mater., 13 (2001) 1131.
56 J. M. Yeh, C. L. Chen, Y. C. Chen, C. Y. Ma, K. R. Lee, Y. Wei and S. Li, Polymer, 43 (2002) 2729.
57 J. M. Yeh, S. J. Liou, C. Y. Lin, C. Y. Cheng, Y. W. Chang and K. R. Lee, Chem. Mater., 14 (2002) 154.
58 I. Pointeau, B. Piriou, M. Fedoroff, M. G. Barthes, N. Marmier and F. Fromage. J. Coll. Inter. Sci., 236 (2001) 252.
59 P. Yu, R. J. Kirkpatrick, B. Poe, P. F. McMillan and X. Cong, J. Am. Ceram. Soc., 82 (1999) 742.
60 Y. H. Yu, C. Y. Lin, J. M. Yeh and W. H. Lin, Polymer, 44 (2003) 3553.
61 B. Chowdhury, J. Therm. Anal. Cal., 78 (2004) 215.
62 M. Drabik, L. Galikova, F. Hanic and J. H. Sharp, Chem. Papers, 51 (1997) 363.
63 M. Drabik, L. Galikova and P. Zimermann, J. Therm. Anal. Cal., 56 (1999) 117.
64 I. Janotka and L'. Krajči, Bul. Mater. Sci., 23 (2000) 521.
65 H. F. W. Taylor, Cement Chemistry, 2nd Edn. (Thomas Telford Publ., London 1998).
66 I. Janotka, L'. Krajči, A. Ray and S.C. Mojumdar, Cem. Concr. Res., 33 (2003) 489.
67 C. A.Strydom and J. H. Potgieter, An investigation into the chemical nature of the reactivity of lime, Proc. 10th Int. Congr. Chem. Cement (Ed. H. Justnes, Sweden 1997).
68 I. Janotka and S. C. Mojumdar, Solid State Phenomena, 90 (2003) 309.
69 I. Janotka, T. Nürnbergerová and L. Nad, Magaz. Concr. Res., 52 (2000) 399.

Received: January 16, 2004
In revised form: February 14, 2005

DOI: 10.1007/s10973-005-6837-y